

## Three-dimensional spin orientation in antiferromagnetic domain walls of NiO studied by x-ray magnetic linear dichroism photoemission electron microscopy

Kuniaki Arai,<sup>1</sup> Taichi Okuda,<sup>2</sup> Arata Tanaka,<sup>3</sup> Masato Kotsugi,<sup>4,5</sup> Keiki Fukumoto,<sup>4,\*</sup> Takuo Ohkochi,<sup>4</sup> Tetsuya Nakamura,<sup>4</sup> Tomohiro Matsushita,<sup>4</sup> Takayuki Muro,<sup>4</sup> Masaki Oura,<sup>6</sup> Yasunori Senba,<sup>4</sup> Haruhiko Ohashi,<sup>4</sup> Akito Kakizaki,<sup>1</sup> Chiharu Mitsumata,<sup>7</sup> and Toyohiko Kinoshita<sup>4,5,†</sup>

<sup>1</sup>*Institute for Solid State Physics, University of Tokyo, Kashiwa, Chiba 277–8581, Japan*

<sup>2</sup>*Hiroshima Synchrotron Radiation Center, Hiroshima University, Higashi-Hiroshima, Hiroshima 739–0046, Japan*

<sup>3</sup>*Department of Quantum Matter, ADSM, Hiroshima University, Higashi-Hiroshima, Hiroshima 739–8530, Japan*

<sup>4</sup>*Japan Synchrotron Radiation Research Institute, Sayo, Hyogo 679–5198, Japan*

<sup>5</sup>*JST-CREST, Kawaguchi, Saitama 332–0012, Japan*

<sup>6</sup>*RIKEN-SPring-8 Center, Sayo, Hyogo 679–5148, Japan*

<sup>7</sup>*Graduate School of Engineering, Tohoku University, Sendai 980–8579, Japan*

(Received 29 November 2011; published 29 March 2012)

A determination of the three-dimensional spin directions in all types of domain walls (DWs) of antiferromagnetic NiO has been successfully performed by photoemission electron microscopy combined with x-ray magnetic linear dichroism (XMLD), both for *s*- and *p*-polarized light. By comparing the azimuthal angle dependence of the XMLD contrast in the DWs with cluster model calculations which include the crystal symmetry and full-multiplet splitting, we determine the spin structures in the {001} T walls, {011} T walls, 120° S walls, and 180° S walls. In some cases, distinct S walls are not formed between two adjacent S domains, and the spin direction changes gradually over a wide range of the S domain structures. In the S walls, the spin direction is parallel to the magnetic easy {111} plane. These spin configurations arise from the large difference in anisotropy energy between the in-plane and out-of-plane directions. Unexpectedly large widths in the several hundred nanometer range were observed for all the DWs. This also shows that NiO has a small magnetocrystalline anisotropy energy. Together with Monte Carlo simulation results, the qualitative phenomena concerning the wall energies are discussed. We further investigated the difference in wall energy between the {001} T wall and the {011} T wall. From the Monte Carlo simulation and an experimental study of heating effects, it is revealed that the {001} T wall energy is smaller than the {011} T wall energy.

DOI: [10.1103/PhysRevB.85.104418](https://doi.org/10.1103/PhysRevB.85.104418)

PACS number(s): 75.25.-j, 75.60.Ch, 78.20.Bh, 78.70.Dm

### I. INTRODUCTION

It is very important to understand domain and domain wall (DW) structures of both ferromagnetic (FM) and of antiferromagnetic (AFM) materials, because macroscopic magnetic phenomena are related to these microscopic structures.<sup>1</sup> From a technological point of view, FM/AFM interface and multilayer systems are now widely utilized for magnetic recording techniques.<sup>2</sup> In order to design devices based on fundamental knowledge, information on such microscopic magnetic structures is crucial. One of the most interesting phenomena is known as the exchange bias, which is combined with the magnetic resistance (MR) effect and utilized in spin-valve recording devices. It is considered that the exchange coupling through AFM substrates and FM thin films is the origin of “pinning” of spins at the interface; therefore, determining the spin structures is essential. Mauri and co-workers suggested how spins are coupled in FM/AFM systems from a calculation,<sup>3</sup> and predicted spin rotation from the substrate to the outermost surface through the interface. Such model calculations rely on knowledge of parameters such as anisotropy, exchange energies, and magnetostatic energies. Therefore, detailed investigation of domain and DW structures of realistic materials is very important.

Here, we focus on the detailed domain and DW structures of NiO, which is a fundamental and typical AFM material with a Néel temperature of  $T_N = 523$  K and a collinear spin

structure. The AFM superexchange interaction of the Ni-O-Ni bonds along the  $\langle 100 \rangle$  directions leads to the formation of FM-ordered {111} planes, where spins in the adjacent {111} planes align in the antiparallel direction, as shown in Fig. 1. Owing to the magnetostriction caused by AFM ordering, the NiO crystal consists of many twinned crystals for temperatures below  $T_N$ . This crystallographic twinning leads to four different domains, i.e., the so-called twin domains (T domains), with four different contractions along the  $\langle 111 \rangle$  axes. In a single T domain, there are three possible spin easy axes along the  $\langle 112 \rangle$  directions. Thus, in total, there are 12 types of spin domains (S domains). This makes the domain structure in NiO very complicated. It has been suggested<sup>4</sup> that domain walls are formed at the boundaries between adjacent domains, in the same way as in FM materials. Figure 2 shows the possible DWs between the T domains. This type of DW is called a T wall. As shown in the figures, two types of DWs exist, i.e., the {001} and {011} T walls. In the same way, S walls are formed between two different S domains. Schematic illustrations of the possible types of S wall are shown in Fig. 3. Because the easy axes of the spin are along the  $\langle 112 \rangle$  directions, the angle of two S domains adjacent to the S wall should be 60° or 120°, as shown in Figs. 3(a) and 3(b). Usually these angles cannot be distinguished because of the AFM nature of spin vectors. However, there is a possibility of the existence of these two types of S walls as described below. As shown in Fig. 3(c), an 180° S wall is formed. In this case, the two S

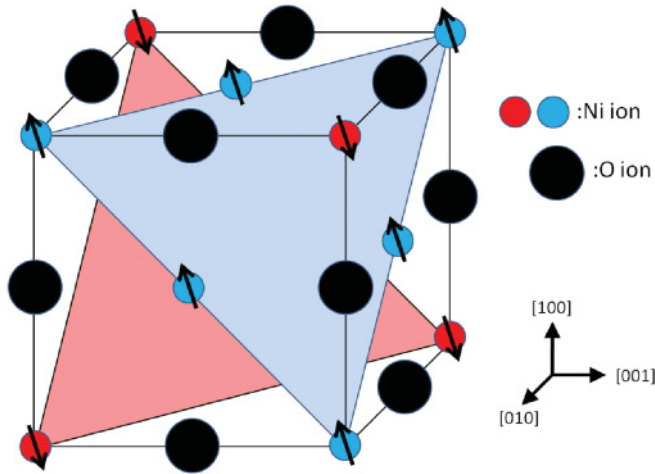


FIG. 1. (Color online) Schematic illustration of the AFM spin structure in NiO. The circles indicate Ni<sup>2+</sup> ions with up and down spins. The spin directions are parallel to the  $[\bar{2}11]$  direction. The black circles indicate O<sup>2-</sup> ions. The spins couple ferromagnetically within the same {111} plane.

domains adjacent to the S wall should be equivalent, having the same spin directions. However, if the {111} planes of the two domains form antiphase coupling beside the S wall as shown in Fig. 3(d), then the 180° S wall can exist, because the each {111} plane has FM nature and a specific spin vector. In the same sense, there may be a difference in the 60° and 120° S walls, if we consider the individual {111} planes beside the walls.

Following the work in the 1960s,<sup>4</sup> there have been several theoretical and experimental studies of the DWs of NiO.<sup>5-11</sup>

However, few microscopic observations with submicrometer resolution have been reported. Weber and co-workers successfully observed the {001} T wall, the 180° S wall, and double-wall structures by a combination of photoemission electron microscope (PEEM) and x-ray magnetic linear dichroism (XMLD) in the soft-x-ray range.<sup>12</sup> They reported wall widths of several hundred nanometers, and showed the AFM spin structures in the {001} T wall. The XMLD-PEEM method using the Ni *L*<sub>2</sub> absorption edge gives high-resolution (~100 nm or less) AFM domain structure images.<sup>13-15</sup> In XMLD-PEEM, the image contrast is sensitive to the angle between the polarization vectors of excitation light and the spin vectors. One can determine therefore the AFM spin vector directions from the contrast by varying the relative orientation of the polarization vector and the sample axis. In Ref. 12, the image of the DW structures was enhanced under the condition of contrast suppression of AFM domains by optimizing the relation of the polarization vector and the sample axis. Although qualitative interpretations of the NiO domain structures following initial reports of those PEEM studies<sup>12-15</sup> were shown, the determination of the spin orientation was not accurate because the crystal symmetry was not considered in the XMLD analyses (only an atomic model was considered). In the atomic model,<sup>16</sup> the XMLD contrast is considered to follow the relation given by the formula

$$\text{XMLD} \propto 3\cos^2\theta - 1, \quad (1)$$

where  $\theta$  is the angle between the magnetization vector and the polarization of the excitation light. The use of formula (1) has now been refuted for the XMLD analyses of NiO.<sup>17-19</sup> Considering the crystal symmetry of NiO for XMLD contrast in the full-multiplet theory, complete assignment of the

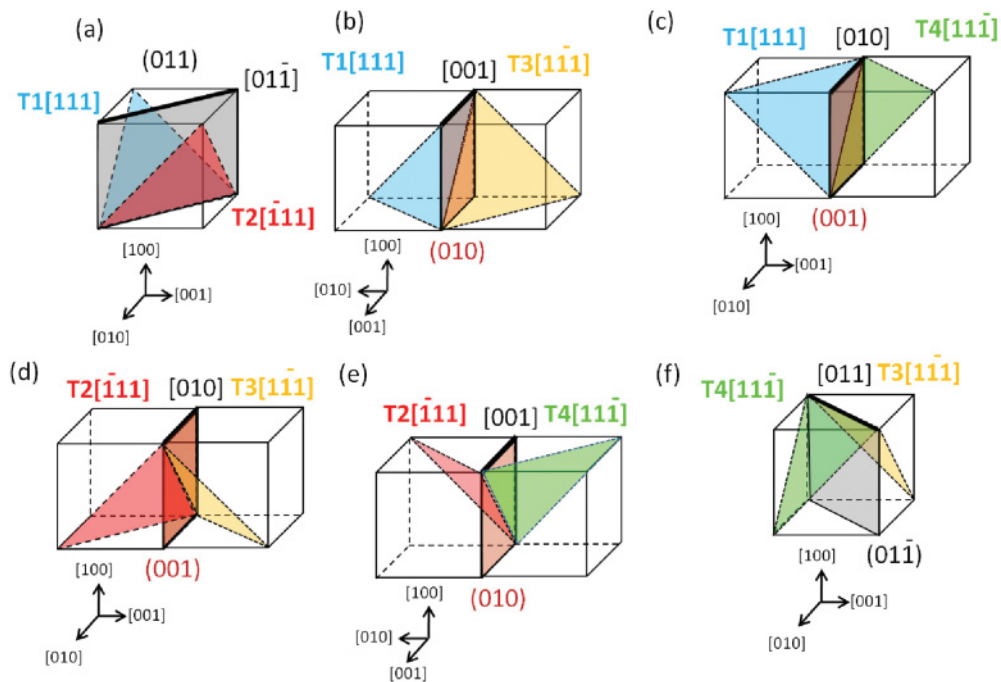


FIG. 2. (Color online) Schematic illustrations of possible types of T walls. (a), (f) {011} T walls, where the walls are formed between T1[111] and T2[111], and T3[111] and T4[111] domains, respectively. (b)–(e) {001} T walls, where the walls are formed between T1–T3, T1–T4, T2–T3, and T2–T4.

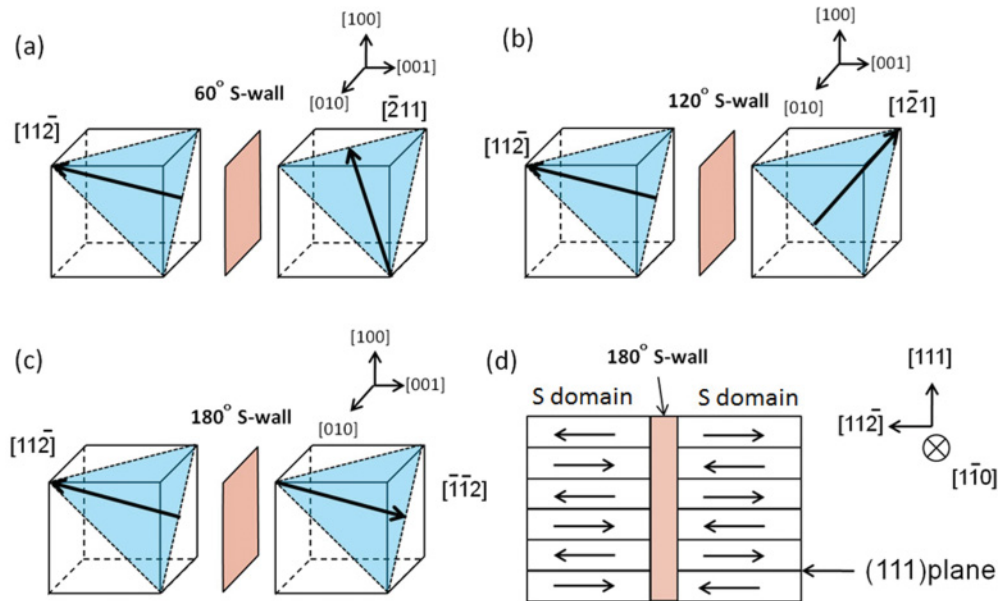


FIG. 3. (Color online) Schematic illustrations of possible types of S walls: (a) 60° S wall, (b) 120° S wall, (c) 180° S wall, and (d) same as in (c) but viewed from the  $[1\bar{1}0]$  direction.

three-dimensional (3D) spin structure in each AFM domain has become possible only very recently.<sup>20</sup> In Ref. 20, change in the XMLD contrast image as a function of azimuthal rotation angle against the polarization vector was carefully compared with a model calculation, leading to a reasonable 3D AFM spin configuration for each domain. In this sense, the investigation of the DWs of NiO in Ref. 12 should be reexamined by using the method proposed in Ref. 20, i.e., considering the crystal symmetry.

In the present study, we have observed the 3D spin structures in all types of AFM DWs of NiO by XMLD-PEEM. The spin directions in the DWs have been determined by comparing the azimuthal angle dependence of the XMLD contrast with a cluster model calculation which includes crystal symmetry and full multiplet splitting. We have also estimated the width of the DWs. From our results, we discuss the DW energy together with a Monte Carlo simulation. By observing changes in the AFM domain structures before and after annealing of the sample, the energy difference between the  $\{001\}$  and  $\{011\}$  T walls is discussed.

## II. EXPERIMENTS AND CALCULATION

### A. Experiments

The crystallographic axes of a NiO single crystal sample were checked by Laue x-ray diffraction. The sample was cleaved at the  $(100)$  plane in atmosphere and then immediately transferred into an ultrahigh-vacuum (UHV) chamber. The crystal orientation was also confirmed by low-energy electron diffraction (LEED) in UHV. The XMLD-PEEM experiments were performed using two PEEM apparatuses at beamlines BL17SU and 25SU at SPring-8. All of the PEEM observations were performed at room temperature. The base pressure of the chambers was  $\sim 7 \times 10^{-8}$  Pa. The apparatus at BL17SU is a spectroscopic photoemission and low-energy electron microscope (SPELEEM).<sup>21</sup> The spatial resolution is better

than  $\sim 70$  nm. (In the best case, we achieved 22 nm.) The beamline provides  $s$  and  $p$  linearly and circularly polarized soft x ray.<sup>22</sup> The degrees of  $s$  and  $p$  polarization are higher than 0.9 and 0.75, respectively, in the photon energy range from 500 to 900 eV. The incident angle of the light from the surface was  $16^\circ$ . We recorded two images at the Ni  $L_2$  edge double peaks  $h\nu = 870.2$  and  $871.3$  eV; see Fig. 1(b) in Ref. 20 and divided one by the other. The obtained image corresponds to the S domain structures as in Ref. 20. In the same way, we could obtain the x-ray nonmagnetic linear dichroism (XLD) image at the O  $K$  edge  $h\nu = 531.4$  and  $532.2$  eV; see Fig. 1(a) in Ref. 20, which reflects the twin-domain (T domain) structure originating from the AFM crystal distortion.<sup>15,23</sup> As discussed in Refs. 20 and 23, the XMLD and XLD contrasts are sensitive to the angle between the polarization vector and the spin axes. In order to deduce the AFM spin axes in each S domain, we have observed the variation of the local contrasts of the XMLD-PEEM images depending on the x-ray incidence angle. For this purpose, the sample is rotated about the surface normal  $[100]$  direction. We refer to this azimuthal angle dependence as AAD hereafter. When the light is incident along  $[001]$  direction, we determine the azimuthal angle as  $0^\circ$ , and along  $[010]$ ,  $90^\circ$ . The assignment of the S domain spin vectors was performed by comparing the AAD contrast ratio of the images with a cluster model calculation (described in Sec. 2.2) which includes the crystal symmetry. The DW structures were also observed in the same way. In some AAD contrast images, we found clear DW structures both for T and S walls. The spin directions of the DWs were also determined from the comparison with the calculation for the corresponding AAD.

In order to investigate the heating effect of the domain and DW structures, we anneal the sample up to a temperature of 540 K, just above  $T_N$ , for about 25 min. The observation was performed at room temperature using the other PEEM apparatus at BL25SU,<sup>24</sup> where a compact PEEM apparatus (ELMITEC PEEMSPECTOR) has been installed.<sup>25</sup> The

circularly polarized soft x-rays were incident on the sample at an angle of  $30^\circ$  from the surface. Although the helical undulator at BL25SU cannot provide linearly polarized light, we can obtain the AFM domain structures (spin domain; S domain) of NiO by using the XMLD effect at the Ni  $L_2$  edge.<sup>25</sup> This is because circularly polarized light can be considered as a coherent superposition of  $s$  and  $p$  linearly polarized light, and the  $s$  and the  $p$  components individually contribute to the XMLD effect but represent the sum of the images for  $s$ - and  $p$ -polarized light. Here both right- and left-circularly polarized light gave the same image contrast. The details of linear dichroism effects for nonlinearly polarized light are described elsewhere.<sup>23,26,27</sup>

### B. Cluster model calculation

To determine the AFM domain structure of NiO, we used an analytic expression, which describes the intensity ratio of the double peak of the linear dichroic x-ray absorption spectra (XAS) at Ni  $L_2$  edge as a function of the polarization vector of the incident light and the direction of the spin magnetic moment at the Ni sites. This expression was derived from the group theory and the configuration-interaction NiO<sub>6</sub> cluster model calculations in our previous work.<sup>20</sup>

The linear dichroic XAS at the transition metal  $L_{2,3}$  edges is sensitive to not only the orbital polarization, but also the direction of the spin magnetic moment at the photoexcited site, because of the large  $2p$  core spin-orbit interaction. Since there is no orbital degree of freedom in the initial state  $3d^8$  ( $^3A_2$ ) configuration of the Ni<sup>2+</sup> ion in NiO, the AAD of the Ni  $L_{2,3}$  XAS can be described by the polarization vector of the incident light  $\boldsymbol{\epsilon}$  and the direction of the magnetic moment  $\boldsymbol{m}$  in the initial state (both are unit vectors). Each final state has a different AAD, and the intensity can be written in a form which is invariant under the  $O_h$  point-group symmetry operations

$$I(\boldsymbol{\epsilon}, \boldsymbol{m}) = C_1 + C_2 F(\boldsymbol{\epsilon}, \boldsymbol{m}) + C_3 G(\boldsymbol{\epsilon}, \boldsymbol{m}),$$

where  $F(\boldsymbol{\epsilon}, \boldsymbol{m}) = (\epsilon_x m_x)^2 + (\epsilon_y m_y)^2 + (\epsilon_z m_z)^2 - 1/3$ ,  $G(\boldsymbol{\epsilon}, \boldsymbol{m}) = 2(\epsilon_y \epsilon_z m_y m_z + \epsilon_z \epsilon_x m_z m_x + \epsilon_x \epsilon_y m_x m_y)$ , and  $C_i$  ( $i = 1, 2, 3$ ) are constants which depend on the final-state multiplet we consider. The Ni  $L_2$  XAS of NiO has a double-peak structure. The NiO<sub>6</sub> cluster model analysis reveals that the high-energy peak located at 871.3 eV arises from a final state with  $T_1$  symmetry, and the low-energy peak positioned at 870.2 eV originates from  $T_2$  and  $E$  final states. From the group theory, the polarization dependence of the intensities of these multiplets can be derived as  $I_{T_1} = C_{T_1}(1/3 + F/4 - G/4)$ ,  $I_{T_2} = C_{T_2}(1/3 + F/4 + G/4)$ , and  $I_E = C_E(2/9 - F/3$

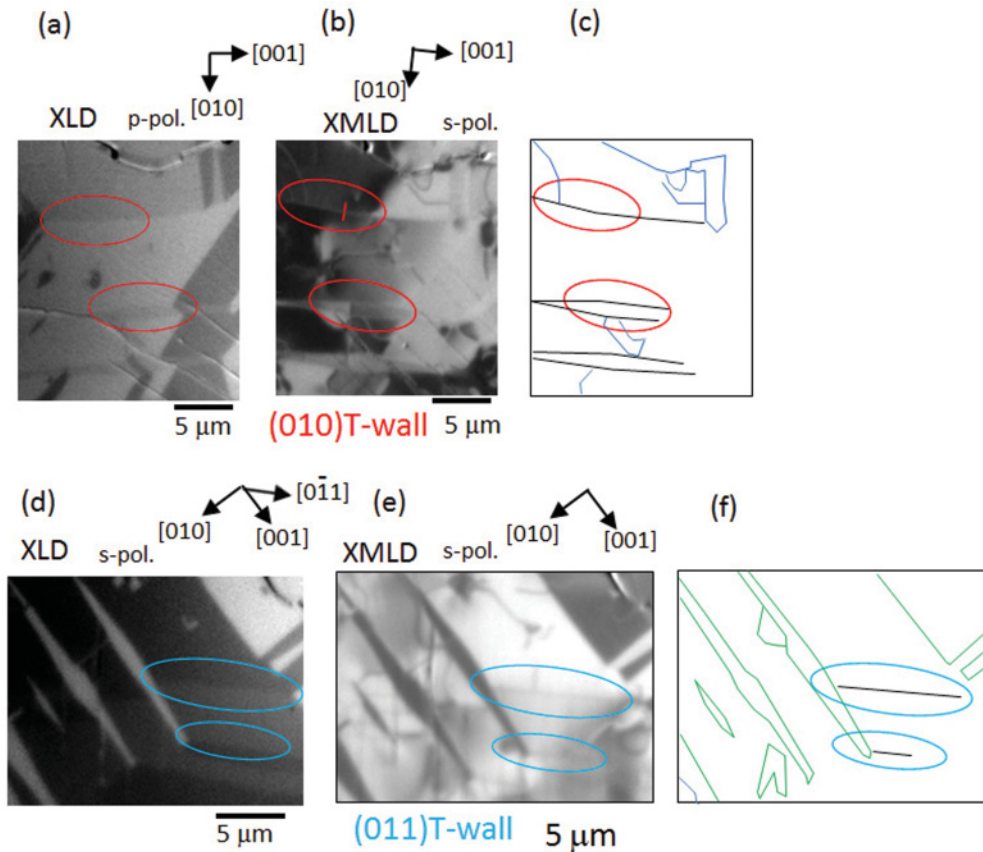


FIG. 4. (Color online) (a) XLD- PEEM image recorded with  $p$ -polarized light at the O  $K$  edge. The T domains of NiO are observed. (010) T walls are located in the areas surrounded by elliptic curves. (b) XMLD image recorded with  $s$ -polarized light at the Ni  $L_2$  edge. The T and S domains of NiO are observed. The observed area is the same as in (a). (010) T walls are located in the areas surrounded by elliptic curves. Along the tick mark, we derived the line profile in Fig. 8. (c) Schematic illustration of (a). (d) Same as in (a) but for a different area, and for  $s$ -polarized light. (011) T walls are located in the areas surrounded by elliptic curves. (e) Same as in (b) but observed at the same area in (d). (011) T walls are located in the areas surrounded by elliptic curves. (f) Schematic illustration of (d).

+  $G/6$ ). The relative intensities can be determined by the cluster model calculations, and ratios  $C_{T1}/C_{T2} = 3.0$  and  $C_{T1}/C_E = 1.0$  are found. From these results the ratio of the high-energy to low-energy peak intensities can be written as  $I_{\text{high}}/I_{\text{low}} = I_{T1}/[I_{T2} + I_E]$ . The effects of peak broadening can be mimicked by replacing the ratio  $I_{\text{high}}/I_{\text{low}}$  by  $(I_{\text{high}} + rI_{\text{low}})/(I_{\text{low}} + rI_{\text{high}})$  with  $r \sim 0.12$ .

### C. Monte Carlo simulation

To understand the spin directions in the magnetic DW qualitatively, we performed a Monte Carlo (MC) simulation using the Heisenberg spin model. The numerical calculation simply used the single-spin-flip Metropolis scheme under the equilibrium occupation probability determined by the Boltzmann distribution. The spin direction was obtained by the thermal average of 40,000 Monte Carlo steps (MCSs) for each spin. Before taking account of thermal average, 15,000 MCSs were performed for thermal relaxation at each temperature. The lattice model used in the MC simulation included  $9 \times 9 \times 4000$  atoms (in order of  $x$ ,  $y$ , and  $z$  coordination) having the simple cube (SC) form, because the sublattice of Ni atoms in NiO corresponds to the SC lattice. For

the magnetic parameters, the exchange constants used were  $J_{12} = -J_{11} = -10$  meV, and the cubic anisotropy constant  $K_1$  was defined from  $J_{11}/K_1 = 1000$ , where  $J_{11}$  and  $J_{12}$ , respectively, dominated the exchange energy in the  $x$ - $y$  plane and  $z$  direction. The value of  $J_{ij}$  was taken from Refs. 28–30. An accurate value of  $K_1$  for antiferromagnetic materials is not available, so we used the value from Ref. 31. Using these values, we applied the periodic boundary condition in the  $x$  and  $y$  directions, and a fixed boundary condition was used in the  $z$  direction. The direction of fixed spin was selected by the observation of the NiO magnetic domain structure.

## III. RESULTS AND DISCUSSION

### A. Spin structures in domain walls

First, we observed the AFM domain structures of bare NiO(100). Both XLD- and XMLD-PEEM images were taken at O  $K$  and Ni  $L_2$  edges, respectively, which reflect the T domain<sup>15,23</sup> and S domain structures. Representative results are shown in Figs. 4 and 5. From the AAD of the XLD contrast at the O  $K$  edge, we notice the shape of T domain boundaries. From the AAD of the XMLD contrast, we could assign the spin directions of the S domain structures, as reported in

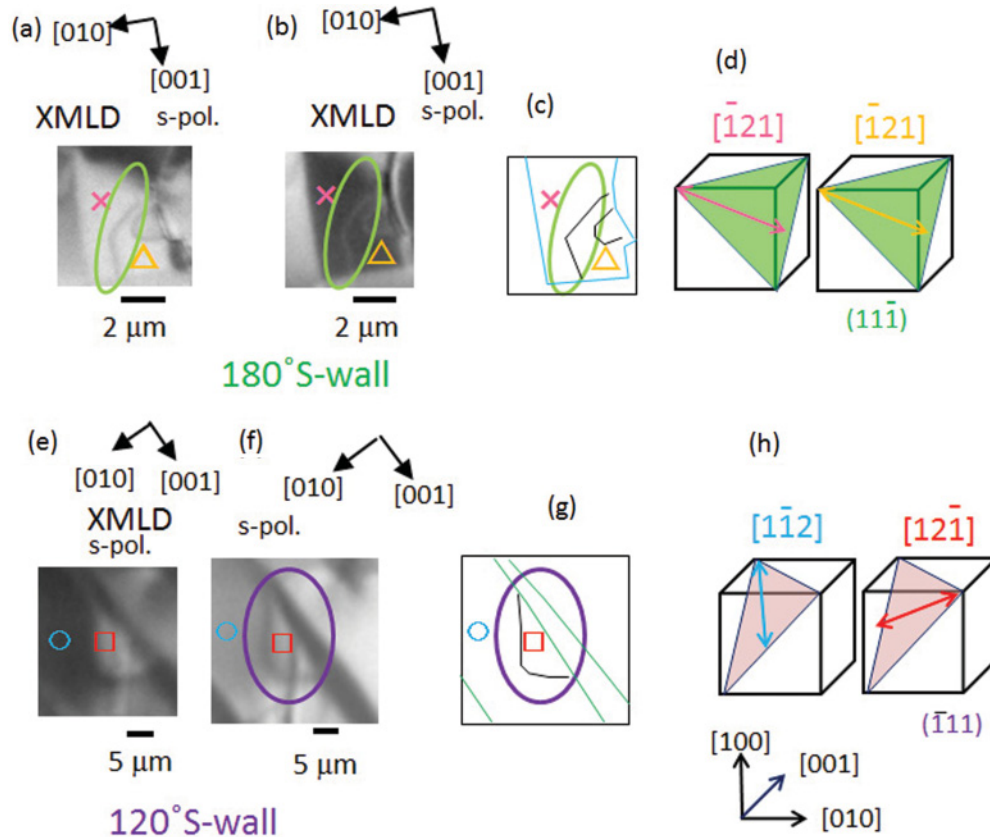


FIG. 5. (Color online) (a) XMLD-PEEM image of NiO recorded with  $s$ -polarized light. The areas marked with a cross and a triangle correspond to S domains with spin axes illustrated in (d). The area surrounded by an elliptic curve is a  $180^\circ$  S wall. The crystallographic axes are also indicated. (b) Same as in (a) but with a different light incidence angle. (c) Schematic illustration of (a) and (b). (d) Schematic illustration of the easy spin axes of the S domains marked by the cross and the triangle S domains in (a)–(c). (e) Same as in (a) but for a different observed area. The areas marked with a circle and a square correspond to S domains with spin axes illustrated in (h). The area surrounded by an elliptic curve is a  $120^\circ$  S wall. (f) Same as in (e) but with a different light incidence angle. (g) Schematic illustration of (e) and (f). (h) Schematic illustration of the easy spin axes of the S domains marked by the cross and the triangle S domains in (e)–(g).

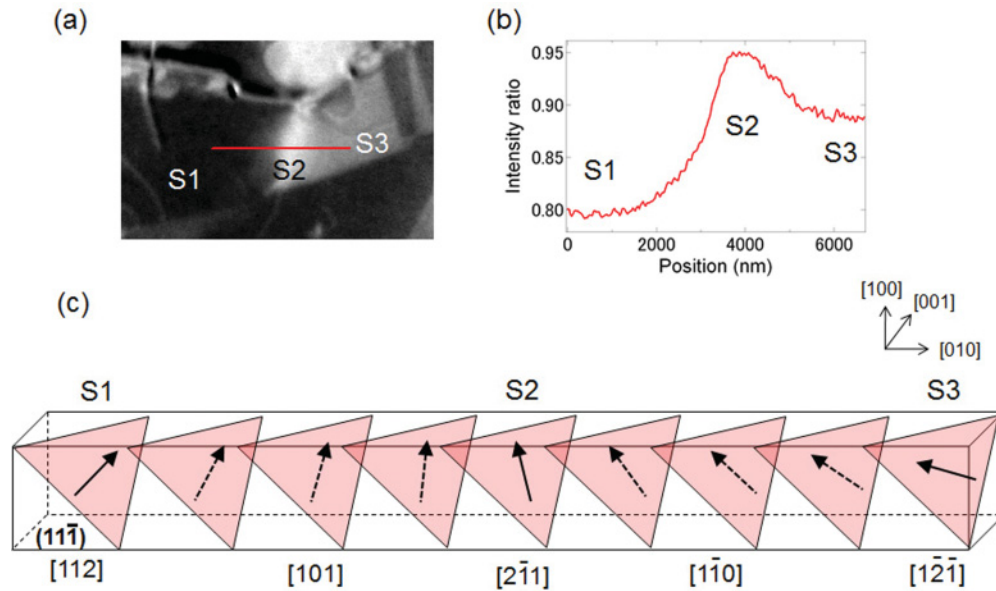


FIG. 6. (Color online) (a) XMLD-PEEM image in a single T domain. Three S domains, S1, S2, and S3, are observed. (b) Line profile of the solid line shown in (a). This corresponds to the contrast along S1 to S2 to S3. (c) Spin structures estimated from the contrast in (a). The spin axes gradually change from S1 to S2 to S3.

Ref. 20. Specifically, in some optimum conditions of azimuthal angles, we observed clear DW structures both between T and S domains, as shown in the area surrounded by ellipses in Figs. 4 and 5. Here, all the types of DW of NiO except for the  $60^\circ$  S wall are successfully observed. For the  $60^\circ$  S wall, distinct wall structures are not formed, as discussed below. The  $\{001\}$  T walls [Figs. 4(a)–4(c)],  $\{011\}$  T walls [Figs. 4(d)–4(f)],  $180^\circ$  S wall [Figs. 5(a)–5(d)], and  $120^\circ$  S wall [Figs. 5(e)–5(h)] are clearly observed. The  $\{001\}$  T wall is situated between two different T domains and runs along the  $[001]$  direction. Here we see brighter contrast in the DW than those of the adjacent S domains in Fig. 4(b). The  $\{011\}$  T wall runs along the  $[0\bar{1}1]$  direction. Here the DW contrast is darker than the adjacent S domains in Fig. 4(e). It is expected that these different DW contrasts should reflect the spin directions in the DWs.

The S domains marked by a cross and a triangle in Fig. 5(a) belong to a single T domain and show the same contrast. When we rotate the sample azimuthally [Fig. 5(b)], the contrast of those two domains becomes darker, but still both domains show the same contrast. This behavior differs from that of the S domains. We calculated all the possible spin orientations of the S domains and found a plausible solution which reproduces the experimental AAD results qualitatively. These two domains, therefore, have the same spin easy axis  $[\bar{1}21]$  (or  $[1\bar{2}\bar{1}]$ ), and the DW observed in Figs. 5(a) and 5(b) is the  $180^\circ$  S wall. In contrast to the fact that the T walls run straight, the S wall does not run straight and has a shape similar to an earthworm.

In the same way, we observed the  $120^\circ$  S wall [see Figs. 5(e) and 5(f)]. Here the spin axes of the S domains adjacent to the S wall, marked by a circle and a square in the figure, are  $[1\bar{1}2]$  (or  $[\bar{1}1\bar{2}]$ ) and  $[1\bar{2}\bar{1}]$  (or  $[\bar{1}\bar{2}1]$ ), respectively. There have been no reports of the detailed observation of  $120^\circ$  S wall so far. Our result is the first successful observation of the  $120^\circ$  S wall. The reason we distinguish this DW as the  $120^\circ$  S wall and not as the  $60^\circ$  S wall is as follows. From the AAD analysis for

this DW, we notice that the spins rotate  $120^\circ$  from the square marked S domain to the circle-marked one (see Fig. 11). The  $120^\circ$  S wall also does not run straight. As discussed below, the magnetocrystalline anisotropy energy is estimated to be very small. Therefore, the spin axes within the  $\{111\}$  planes easily change directions from the easy  $\langle 112 \rangle$  axes. This is one reason the S walls do not run straight.

Figure 6(a) also shows the XMLD image at the Ni  $L_2$  edge but for a different place from Figs. 4 and 5. Here we observe three kinds of contrast corresponding to the three types of S domains, S1, S2, and S3. The line profile of the contrast change from S1 to S3 is shown in Fig. 6(b). It is noticed that the contrast gradually changes from S1 to S2, and then S2 to S3. No distinct contrast jump corresponding to DW structure is observed. We schematically illustrate our model, showing how the spins rotate in this region in Fig. 6(c). The calculated AAD based on the model in Fig. 6(c) reproduces the line profile in Fig. 6(b). It can be seen that spins rotate from  $[112] \rightarrow [101] \rightarrow [1\bar{2}\bar{1}] \rightarrow [1\bar{1}0] \rightarrow [1\bar{2}\bar{1}]$  gradually within the  $\{111\}$  plane. Therefore, if the angle between the adjacent two S domains is  $60^\circ$ , no distinct S wall is formed. This phenomenon can be explained again by the small magnetocrystalline anisotropy energy within the  $\{111\}$  planes. The reason there are two types of DWs is not clear, but it is probably related to the arrangement of the surrounding domains and spin structures. This means that spins easily rotate within  $\{111\}$  planes. For an angle of  $120^\circ$ , the formation of DWs is energetically stable, whereas spin rotations easily happen with an angle of  $60^\circ$ . Depending on the arrangement, the magnetocrystalline energy may show frustration and become complicated, leading to a variety of domains and DW arrangements.

Next we assign the spin directions of each DW structure presented in Figs. 4 and 5. We show here how we determine the spins in the  $\{001\}$  T wall as a representative example. Figures 7(a)–7(e) show the AAD of the XMLD images at

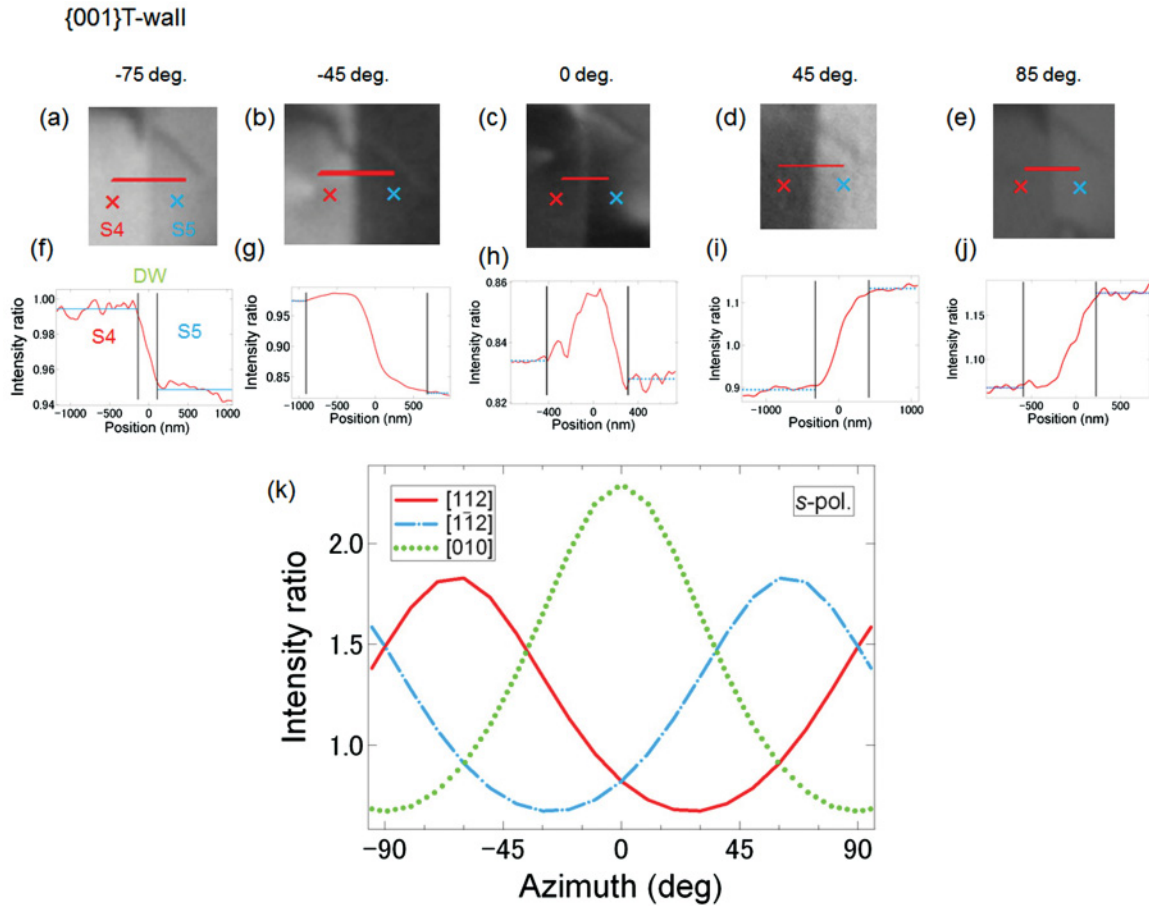


FIG. 7. (Color online) AAD of one of the {001} T walls. (a)–(e) XMLD-PEEM images for different azimuthal angles but the same observed area. The cross and the triangle areas are S4 and S5 domains. The image was recorded using *s*-polarized light. (f)–(j) Line profiles for the solid lines shown in (a)–(e). These correspond to the contrast for S4 and S5 domains and DW. (k) Calculated AAD for three kinds of spin axes. These are calculated for the axes which can reproduce the observed AAD above.

the Ni  $L_2$  edge for *s*-polarized light, and the {001} T walls are clearly observed. Beside the T wall, two kinds of S domains exist, and these are marked by crosses and triangles in the figures. The line profiles from the S4 (cross) to S5 (triangle) domains for each azimuthal angle are indicated in Figs. 7(f)–7(i). Because the wall width is much smaller than the size of the domains, and because of the limitation of the spatial resolution, the absolute contrast within the DW cannot be correctly estimated, especially at the DW contrast in the dark region at the line profiles of (f) and (j). The background subtraction is particularly difficult in the DW region. Furthermore, the experimental azimuthal angles could not be determined so precisely. However, as shown in Figs. 7(a) and 7(e), the DW shows darker contrast than those of the two adjacent S domains. In Figs. 7(c) and 7(h), we see brighter DW contrast than those of the S domains. In Figs. 7(b), 7(d), 7(g), and 7(i), the contrast of the DW is intermediate to those of the adjacent S domains. We can qualitatively note here that these trends in DW contrast. From a comparison between the experimental and calculated AADs, we assign the spin directions of the S domains as  $[112]$  and  $[1\bar{1}2]$ , respectively, as shown in Fig. 7(k). Furthermore, at the center of the DW, the spin vector should be located just in the middle of the spin vectors  $[112]$  and  $[1\bar{1}2]$ . We calculated the AAD of the

XMLD for all the possible vectors and obtained the results shown in the green curve of Fig. 7(k). The most plausible spin vector is  $[010]$ , which reproduces the above tendency of the AAD of the DW contrast. For the other spin directions, we cannot reproduce the AAD tendency above. This result is qualitatively consistent with the analysis for the *p*-polarized light (not shown here).

In addition to this analysis, we confirmed the results by observing the line profile as shown in Fig. 8 derived from Fig. 4(b). If the spin direction at the center of the DW is  $[010]$  as shown in Fig. 8(a), spins within the DW should rotate as in Fig. 8(c), in which the projected spin directions to the (001) surface expected for the rotation are schematically illustrated. The calculated AAD [the solid curve in Fig. 8(b)] is almost consistent with that for the experimental line profile.

In the same manner, we assign the spin directions of all the other DWs as shown in Figs. 9–11. Figure 9 indicates the schematic illustration of the spin directions in the {011} T walls. The directions could not be determined uniquely but are assigned as  $[m12]$  ( $8 \leq m \leq 30$ ). This direction is almost parallel to the  $[100]$ . The direction is perpendicular to the surface, in contrast to the parallel spin direction to the surface observed for the {001} T wall. This difference is due to the difference in magnetoelastic effect between the two T walls.

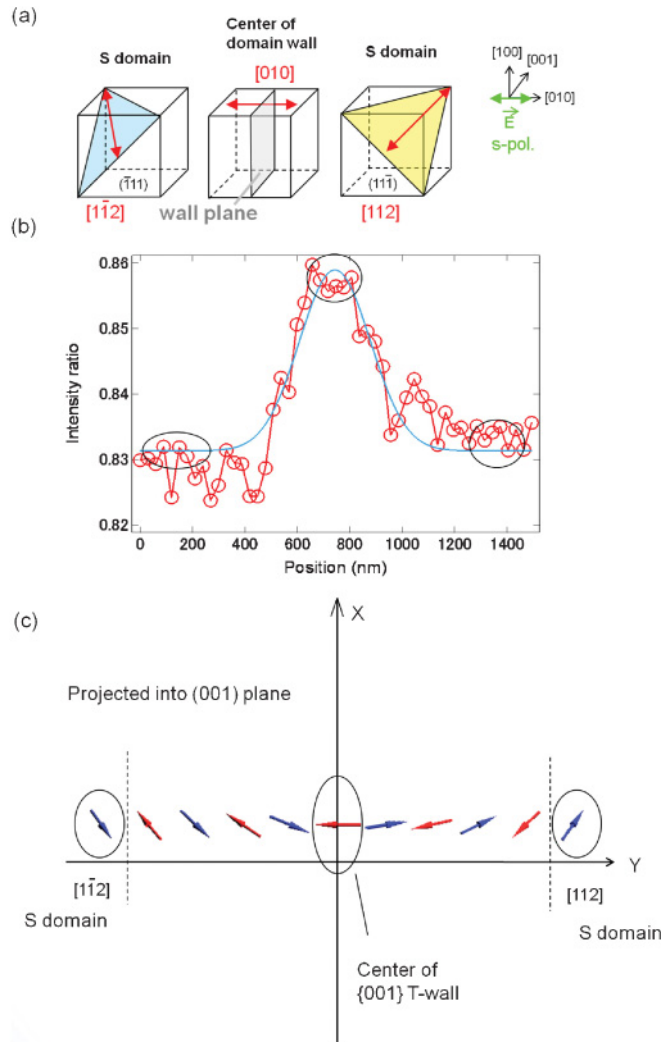


FIG. 8. (Color online) (a) Schematic illustration of the spin structures of {001} T walls obtained by a comparison of the theoretical and experimental AADs. (b) The circles are the experimental line profile of Fig. 4(b). The solid line corresponds to the XMLD contrast calculated for the spin axes shown in (c). (c) Schematic illustration of the spin structures in the {001} T wall shown in (a). Here the axes are projected onto the (001) plane.

We found that there are two types of 180° S wall, as shown in Figs. 10(a) and 10(b). The projection of the spin vectors in the S domains in (a) is larger than those in (b). It can be seen that the spins rotate within the {111} plane in both cases. The situation is also similar for the 120° S walls shown in Figs. 11(a) and 11(b), where the spins rotate 120° within the {111} plane. The rotation within the {111} plane is explained by the large difference in the magnetocrystalline anisotropy energy between the in- and out-of {111} plane directions.

The directions of spin in DWs are calculated by MC simulations and are compared with the observed results shown in Figs. 8 and 9. The spin vectors at the center of DW become [010] and  $[\bar{1} 10 \bar{6}]$  for the {001} T wall and {011} T wall, respectively. The former vector reproduces the observed DW structure; however, the latter one does not agree to the measurement. In these cases, only simple cubic anisotropy is assumed. The simulated spins approximately agree to the

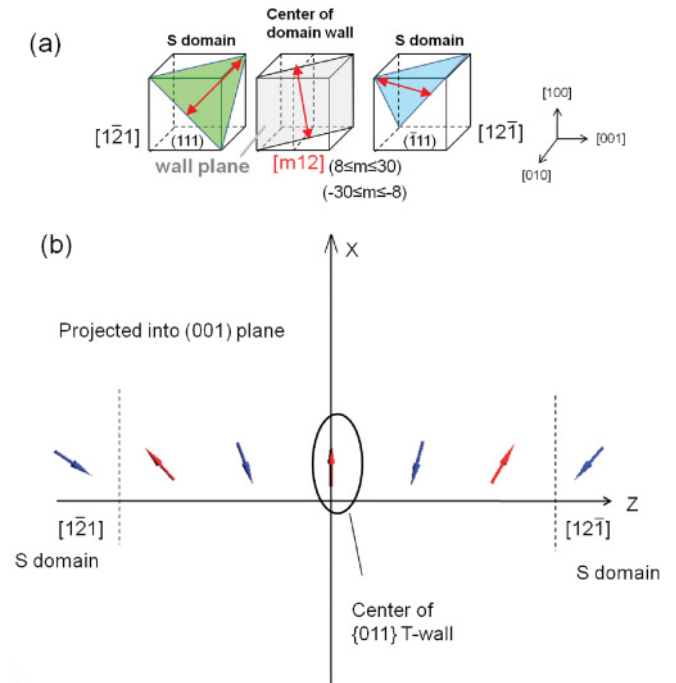


FIG. 9. (Color online) (a) Same as in Fig. 8(a) but for the {011} T wall. (b) Same as in Fig. 8(c) but for the {011} T wall.

vector of  $(\mathbf{b}_R - \mathbf{b}_L)/2$ , where  $\mathbf{b}_R$  and  $\mathbf{b}_L$  are given by the direction of spins at the boundary of DW as shown in Figs. 8 and 9 (namely,  $\mathbf{b}_R$  and  $\mathbf{b}_L$  correspond to the spin vectors of the adjacent two domains). The spin rotation from the direction of  $\mathbf{b}_R$  to  $\mathbf{b}_L$  through  $(\mathbf{b}_R - \mathbf{b}_L)/2$  corresponds to the least amount of exchange energy. Therefore, the exchange energy in the DW should increase, if the spin vector at the center of the DW disagrees to  $(\mathbf{b}_R - \mathbf{b}_L)/2$ . The increased exchange energy needs to be compensated by the reduction of anisotropy energy, because the exchange and anisotropy energies have been taken into account only for the formation of DW in the present model. Otherwise, the deflection of spin cannot be realized. In this sense, the spin structure of the {001} T wall can be formed without strong influence of the magnetic anisotropy. On the other hand, the difference between the vector  $[\bar{1} 10 \bar{6}]$  and  $(\mathbf{b}_R - \mathbf{b}_L)/2$  suggests the necessity of the effect of magnetic anisotropy in the {011} T wall. Furthermore, the MC simulation cannot reproduce the S wall spin directions (results are not shown here). Different from the observed results, these spin directions are not in the {111} plane. This also suggests the necessity of considering the effect of magnetic anisotropy within the (111) plane.

As mentioned above, the discrepancy of the calculated spin vector from the measured result is possibly corrected by introducing the additional anisotropy energy. This additional anisotropy could be realized due to the magnetoelastic effect. However, in this model, the magnitude of anisotropy and the magnetic easy direction for a magnetoelastic interaction are hardly discussed, because the arbitrary parameter settings can be applied to fix the spin vector at the center of DW. Therefore, pointing out the difference between the simple model and the experiments is a limitation of this paper.

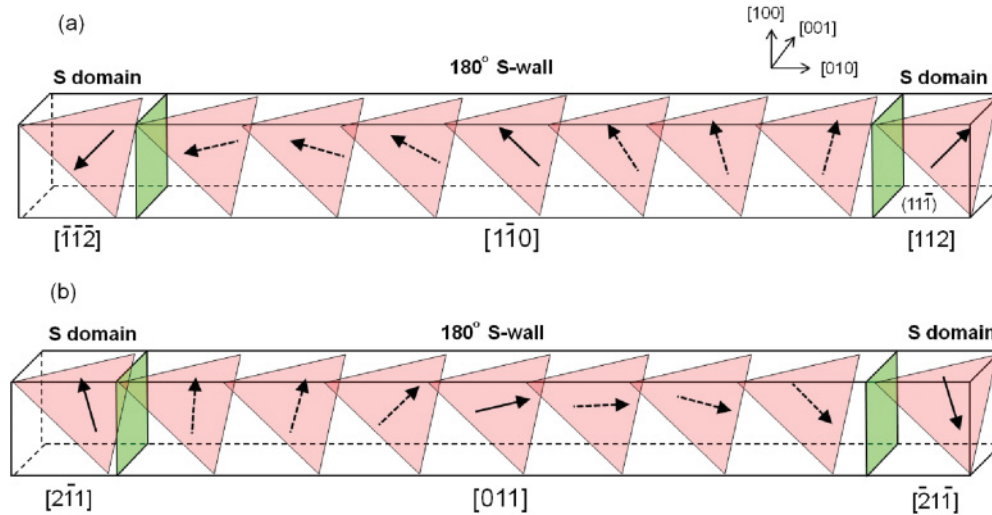


FIG. 10. (Color online) (a) Schematic illustration of the spin structures in one of the  $180^\circ$  S walls obtained from a comparison of the theoretical and experimental AADs. (b) Same as in (a) but for a different type of  $180^\circ$  S wall.

**B. Width of the domain walls**

In this section we discuss the wall widths of the  $\{001\}$  T wall,  $\{011\}$  T wall,  $180^\circ$  S wall, and  $120^\circ$  S wall. As shown in Fig. 8(b), we can obtain the values of DW widths from the line profiles of the XMLD images. The full width of the DW in Fig. 8(b) is estimated to be about 530 nm. This is much larger than that predicted previously.<sup>6</sup> One may wonder whether the values are intrinsic, because PEEM images include information not only from the topmost surface, but also from deeper regions. As shown in Fig. 2, the T walls are situated perpendicular to the (100) surface. Therefore, the observed values for the T walls are intrinsic. In contrast, the S walls may not be situated perpendicular to the (100) surface. The situation is explained in Fig. 12 for the  $180^\circ$  S wall case. It can be understood from the figure that the observed full width includes additional factors which increase the values, such as the DW running obliquely to the surface, and the effect

that PEEM is sensitive to electrons deeper than the outermost surface ( $\sim 10$  nm). Considering such effects, the intrinsic value of the DW width can be expected to be about 80% of the observed one. The extremely large DW width is thus not due to the experimental resolution of better than  $\sim 70$  nm. In the same experimental setup as the present study, we recently observed the DW of FM wire, but a distinct DW width could not be observed.<sup>32</sup> Thus the spatial resolution is good enough for the observation of several hundred nanometer width. Therefore, it is concluded that such large DW widths are intrinsic for NiO. Weber and co-workers<sup>12</sup> also observed the DW width and reported widths of similar magnitude to the present results. We observed a number of DWs and measured their wall widths. Figure 13 shows a histogram of the wall width distributions for four types of wall. Although the distribution is large, the trend in DW width is  $\{011\}$  T wall  $>$   $\{001\}$  T wall, and  $180^\circ$  S wall  $<$   $120^\circ$  S wall. This relationship is due to the difference in wall energy, as discussed below.

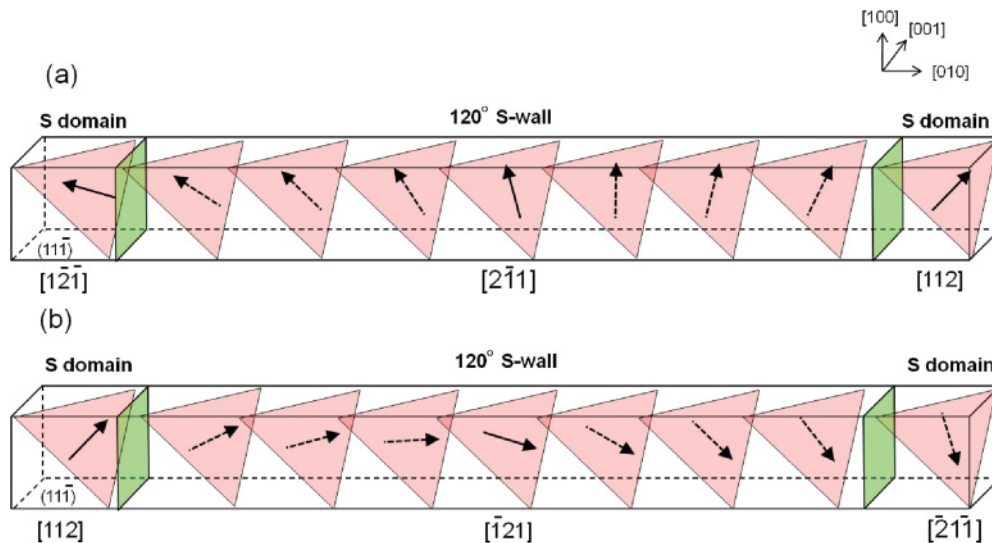


FIG. 11. (Color online) (a) Same as in Fig. 10 but for one of the  $120^\circ$  S walls. (b) Same as in (a) but for a different type of  $120^\circ$  S wall.

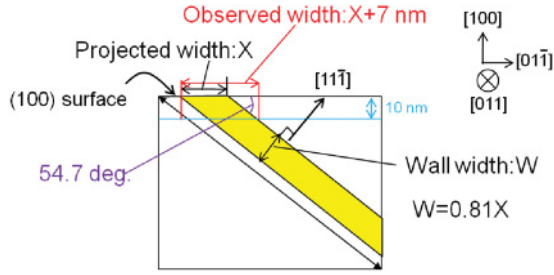


FIG. 12. (Color online) Schematic illustration to explain the difference between the intrinsic DW width and the observed width. This is for a 180° S wall.

The simulated DW width becomes 55 monolayers (MLs; 1 ML ~ 0.3 nm), 100 MLs, 60 MLs, and 75 MLs, respectively, for the {001}, T wall, {011}, T wall, 180° S wall and 120° S wall. The tendency of the simulated width shows {011}, T wall > {001}, T wall, and 180° S wall < 120° S wall. The magnitude relations of DW width both in T domains and in S domains agree with the results in Fig. 13. However, the absolute values of the simulated DW widths are smaller than those of the measured DWs. This difference between measurement and simulation should be discussed carefully.

As discussed in Sec. III A, the deviation from a vector of  $(\mathbf{b}_R - \mathbf{b}_L)/2$  requires an increase in exchange energy. Thus, the reduction of the magnetic anisotropy energy should be achieved in the DW. In other words, an increase in exchange energy has to be matched by a decrease in anisotropy energy. On the other hand, in general, the DW width is proportional to the square root of the exchange energy and is inversely proportional to the square root of the anisotropy energy. The arbitrary antiferromagnetic DWs also correspond to this general principle.<sup>33</sup> Therefore, the large DW width can be created by a large exchange energy or a small anisotropy

energy. As described above, the required relations between the exchange and anisotropy energies are inconsistent with the observed spin vector directions and large DW widths. In addition, the exchange constants  $J_{11}$  and  $J_{12}$  are dominated by the NiO Néel temperature, and these may not be changed in the simulation. To solve this discrepancy, it is thought that the geometric spin frustration owing to the addition of an exchange coupling relatively reduces the influence of exchange energy against the anisotropy. For example, superexchange through the O ion or the third-nearest-neighboring site could possibly introduce geometric spin frustration. Also, the expansion of the model to the polycrystalline potentially includes geometric spin frustration at the grain boundary. The influence of the geometric spin frustration will be discussed in a separate paper.

### C. Heating effects on the T wall and T domain structures

We have investigated the change in T domain structures during annealing. Figure 14 shows comparative XMLD images before (a) and after (c) annealing above  $T_N$ . To guide the eye a schematic illustration of the domains is shown. It can be seen from Figs. 14(a) and 14(b) that most of the T walls run along both the  $\langle 001 \rangle$  and  $\langle 011 \rangle$  directions. After annealing, the number of {011} T walls decreased and the number of {001} T walls increased, as shown in Figs. 14(c) and 14(d). The sample was annealed several times until the domain structures did not change anymore. It can be expected that any strain resulting from the cleaving process is released by annealing. The fact that the number of {001} T walls increases and the number of {011} T walls decreases is that the {001} T wall energy is smaller than that of {011} T wall energy. This is consistent with the MC simulation.

In general, annealing influences the stress and the elastic energy of the crystal, but a study of the elastic properties is outside the scope of this paper. Thus, we simply evaluate the

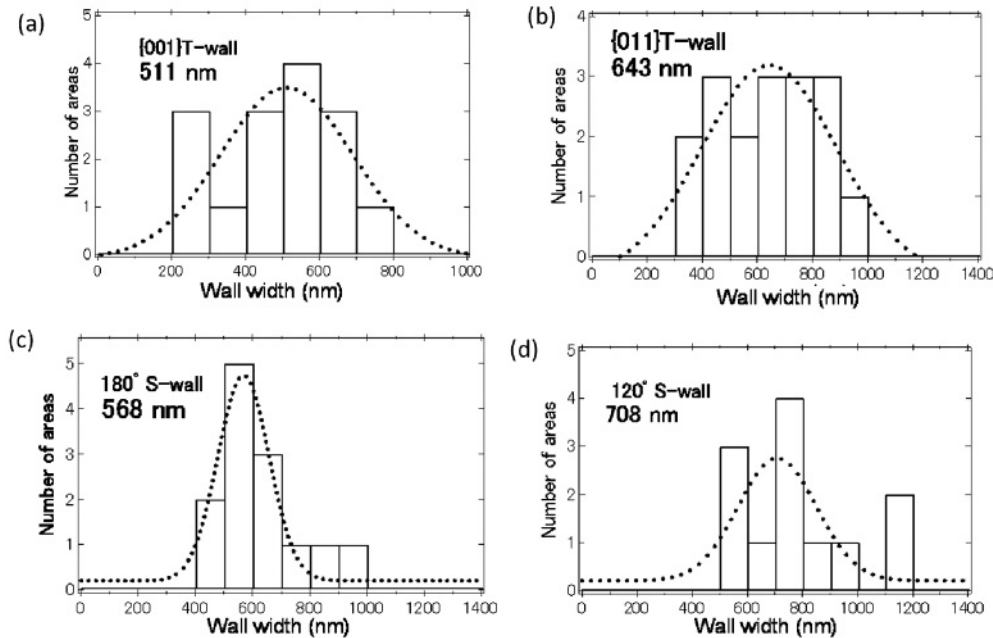


FIG. 13. Distribution of DW widths obtained from many PEEM images. Histograms (a)–(d) correspond to the width distribution for the {001} T wall, {011} T wall, 180° S wall, and 120° S wall, respectively.

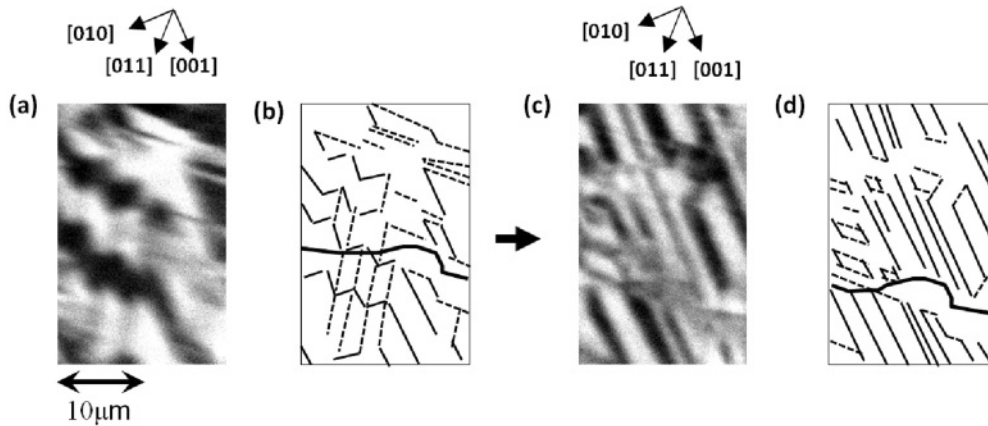


FIG. 14. (a) T and S domain structures of NiO before annealing the sample. The image was recorded using XMLD-PEEM at the Ni  $L_2$  edge. Because circularly polarized light is used, the image corresponds to the sum of images for  $s$ - and  $p$ -polarized light. (b) Schematic illustration of (a). The thick line indicates a surface crack. The solid and dotted lines indicate  $\{001\}$  and  $\{011\}$  T walls, respectively. (c) As in (a) but after annealing at a temperature above  $T_N$  for longer than 25 minutes. (d) Schematic illustration of (c).

thermal stability of the DW. The MC simulations are carried out under the temperature range from  $0.15T_N$  to  $0.75T_N$ , where  $T_N$  is the Néel temperature of modeled NiO. For the  $\{001\}$  T wall, the DW stably shows the structure shown in Fig. 8 for  $T = 0.15T_N$ ,  $0.30T_N$ , and  $0.45T_N$ . Then, the DW width increases at  $T = 0.15T_N$  without significant change of spin arrangement in the DW. Finally, the DW structure is destroyed at  $T = 0.75T_N$ . In contrast, for the  $\{011\}$  T wall, the DW structure is unchanged for  $T = 0.15T_N$ ,  $0.30T_N$ . However, it suddenly breaks down at  $T = 0.45T_N$  without the elongation of DW width before the structural transition. Based on these simulations, the thermal stability of the  $\{001\}$  T wall is higher than that of the  $\{011\}$  T wall.

#### IV. CONCLUSION

We have observed detailed 3D spin structures in all types of DW for AFM NiO(100) by XMLD-PEEM. By comparing the AAD of the XMLD contrast in the DWs for  $s$ - and  $p$ -polarized light with cluster model calculations which include the crystal symmetry and full-multiplet splitting, the spin directions in the  $\{001\}$  T walls,  $\{011\}$  T walls,  $120^\circ$  S walls, and  $180^\circ$  S walls have been determined, although those in the  $\{011\}$  T wall have not been uniquely confirmed. We did not find any distinct  $60^\circ$  S walls. Instead, the spin directions were found to gradually change over a wide range of S domain

structures. The spin directions of the S walls align within the  $\{111\}$  planes, corresponding to the anisotropy energy in the magnetic easy plane being much smaller than that of the out of plane. We also showed the differences in wall widths for all the DWs. Unexpected large widths in the several hundreds of nanometers range were observed for all the DWs. These large widths arise from the small magnetocrystalline anisotropy energy of NiO. Together with Monte Carlo simulation results, the phenomena concerning the wall energy are qualitatively discussed. Annealing the sample above the Néel temperature, the number of  $\{011\}$  T walls decreases and the number of  $\{001\}$  T walls increases. This means that the wall energy of  $\{011\}$  is larger than that of  $\{001\}$ . These findings are important for understanding the fundamental basis of AFM materials and can be expected to be useful for applications to exchange coupled systems.

#### ACKNOWLEDGMENTS

The experiments were performed with the approval of JASRI (Proposals No. 2007A1835, No. 2008A1723, No. 2008A1726, and No. 2009A1667). This research was partially supported by a Grant-in Aid for Scientific Research (S, No. 18101004) from the Japan Society for the Promotion of Science. K.A. and T.K. thank K. Fukamichi, H. Matsuyama, and K. Nakamura for encouragement and useful discussions.

\*Present address: Department of Material Science, Tokyo Institute of Technology, 152-8550, Tokyo, Japan.

†toyohiko@spring8.or.jp

<sup>1</sup>See, for example, “*Magnetic Domains*,” edited by A. Hubert and R. Schäfer (Springer, Berlin, 1998).

<sup>2</sup>J. Nogués and I. K. Schuller, *J. Magn. Magn. Mater.* **192**, 203 (1999).

<sup>3</sup>D. Mauri, H. C. Siegmann, P. S. Bagus, and E. Kay, *J. Appl. Phys.* **62**, 3047 (1987).

<sup>4</sup>W. L. Roth, *J. Appl. Phys.* **31**, 2000 (1960).

<sup>5</sup>S. Saito, M. Miura, and K. Kurosawa, *J. Phys. C* **13**, 1513 (1980).

<sup>6</sup>T. Yamada, *J. Phys. Soc. Jpn.* **21**, 650 (1966).

<sup>7</sup>T. Yamada, S. Saito, and Y. Shimomura, *J. Phys. Soc. Jpn.* **21**, 672 (1966).

<sup>8</sup>M. Ando, *Phys. Status Solidi A* **24**, 473 (1974).

<sup>9</sup>K. Namikawa and K. Terui, *Jpn. J. Appl. Phys.* **23**, 1586 (1984).

- <sup>10</sup>I. Sanger, V. V. Pavlov, M. Bayer, and M. Fiebig, *Phys. Rev. B* **74**, 144401 (2006).
- <sup>11</sup>J. N. Armstrong, M. R. Sullivan, and H. D. Chopra, *Phys. Rev. B* **80**, 104429 (2009).
- <sup>12</sup>N. B. Weber, H. Ohldag, H. Gomonaj, and F. U. Hillebrecht, *Phys. Rev. Lett.* **91**, 237205 (2003).
- <sup>13</sup>F. U. Hillebrecht, H. Ohldag, N. B. Weber, C. Bethke, U. Mick, M. Weiss, and J. Bahrtdt, *Phys. Rev. Lett.* **86**, 3419 (2001).
- <sup>14</sup>H. Ohldag, A. Scholl, F. Nolting, S. Anders, F. U. Hillebrecht, and J. Stohr, *Phys. Rev. Lett.* **86**, 2878 (2001).
- <sup>15</sup>T. Kinoshita, T. Wakita, H.-L. Sun, T. Tohyama, A. Harasawa, H. Kiwata, F. U. Hillebrecht, K. Ono, T. Matsushita, M. Oshima, N. Ueno, Y. Saitoh, and T. Okuda, *J. Phys. Soc. Jpn.* **73**, 2932 (2004).
- <sup>16</sup>D. Alders, J. Vogel, C. Levelut, S. Peacor, T. Himba, M. Sacchi, L. Tjeng, G. van der Laan, B. T. Thole, and G. A. Sawatzky, *Europhys. Lett.* **32**, 259 (1995).
- <sup>17</sup>I. P. Krug, F. U. Hillebrecht, M. W. Haverkort, A. Tanaka, L. H. Tjeng, H. Gomonay, A. Fraile-Rodriguez, F. Nolting, S. Cramm, and C. M. Schneider, *Phys. Rev. B* **78**, 064427 (2008).
- <sup>18</sup>E. Arenholz, G. van der Laan, and F. Nolting, *Appl. Phys. Lett.* **93**, 162506 (2008).
- <sup>19</sup>G. van der Laan, N. D. Telling, A. Potenza, S. S. Dhesi, and E. Arenholz, *Phys. Rev. B* **83**, 064409 (2011).
- <sup>20</sup>K. Arai, T. Okuda, A. Tanaka, M. Kotsugi, K. Fukumoto, M. Oura, Y. Senba, H. Ohashi, T. Nakamura, T. Matsushita, T. Muro, A. Kakizaki and T. Kinoshita, *J. Phys. Soc. Jpn.* **79**, 013703 (2010); **79**, 038001 (2010).
- <sup>21</sup>F. Z. Guo, T. Muro, T. Matsushita, T. Wakita, H. Ohashi, Y. Senba, T. Kinoshita, K. Kobayashi, Y. Saitoh, T. Koshikawa, T. Yasue, M. Oura, T. Takeuchi, and S. Shin, *Rev. Sci. Instrum.* **78**, 066107 (2007).
- <sup>22</sup>M. Oura, T. Nakamura, T. Takeuchi, Y. Senba, H. Ohashi, K. Shirasawa, T. Tanaka, M. Takeuchi, Y. Furukawa, T. Hirono, T. Ohata, H. Kitamura, and S. Shin, *J. Synchrotron Radiat.* **14**, 483 (2007).
- <sup>23</sup>K. Arai, T. Okuda, A. Tanaka, M. Kotsugi, K. Fukumoto, T. Ohkouchi, F. Z. Guo, T. Nakamura, T. Matsushita, T. Muro, M. Oura, Y. Senba, H. Ohashi, A. Kakizaki, and T. Kinoshita (unpublished).
- <sup>24</sup>T. Muro, T. Nakamura, T. Matsushita, T. Wakita, K. Fukumoto, H. Kimura, T. Hirono, T. Kinoshita, T. Hara, K. Shirasawa, M. Takeuchi, and H. Kitamura, *AIP Conf. Proc.* **879**, 571 (2007).
- <sup>25</sup>K. Arai, T. Okuda, A. Tanaka, K. Fukumoto, T. Hasegawa, T. Nakamura, T. Matsushita, T. Muro, A. Kakizaki, and T. Kinoshita, *J. Appl. Phys.* **110**, 084306 (2011).
- <sup>26</sup>We confirmed experimentally that the sum of the XMLD images at the Ni  $L_2$  edge by  $s$ - and  $p$ -polarized light correspond to the image by circularly polarized light at the other beamline BL17SU in SPring-8.
- <sup>27</sup>The similar linear dichroism effect was also observed by using unpolarized ultraviolet light. See F. Z. Guo, H.-L. Sun, T. Okuda, K. Kobayashi, and T. Kinoshita, *Surf. Sci.* **601**, 4686 (2007); G. K. L. Marx, H. J. Elmers, and G. Schonhense, *Phys. Rev. Lett.* **84**, 5888 (2000).
- <sup>28</sup>M. Hutchings and E. J. Samuelsen, *Phys. Rev. B* **6**, 3447 (1972).
- <sup>29</sup>L. C. Bartel and B. Morosin, *Phys. Rev. B* **3**, 1039 (1971).
- <sup>30</sup>J. Milano, L. B. Steren, and M. Grimsditch, *Phys. Rev. Lett.* **93**, 077601 (2004).
- <sup>31</sup>C. Mitsumata, A. Sakuma, and K. Fukamichi, *Phys. Rev. B* **68**, 014437 (2003).
- <sup>32</sup>N. Ohshima, T. Koyama, H. Tanigawa, M. Kotsugi, T. Ohkouchi, D. Chiba, T. Kinoshita, and T. Ono, *J. Phys.: Condens. Matter* **23**, 382202 (2011).
- <sup>33</sup>C. Mitsumata, A. Sakuma, K. Fukamichi, M. Tsunoda, and M. Takahashi, *J. Phys. Soc. Jpn.* **77**, 044602 (2008).